Supporting Information for Rapid Hydrogen–Deuterium Exchange in Liquid Droplets

Erik T. Jansson,[†,‡] Yin-Hung Lai,[‡] Juan G. Santiago,[¶] and Richard N. Zare[*,‡]

†*Department of Chemistry — BMC, Uppsala University, SE-751 24, Uppsala, Sweden*
‡*Department of Chemistry, Stanford University, Stanford, CA 94305, USA*
¶*Department of Mechanical Engineering, Stanford University, Stanford, CA 94305, USA*

E-mail: zare@stanford.edu

Abstract

The supporting information presented here provides information on materials and methods. Notes are given for a description of the spray geometry and velocity field calculation, and the mathematical model for the calculated chemical rate constants.

List of Figures

Materials and methods

Chemicals

Angiotensin I, phenethylamine (Fig. S-1), choline, choline-d_9, and 99.9% D_2O was purchased from Sigma-Aldrich (St. Louis, MO). LC-grade water was purchased from Thermo Fisher Scientific (Waltham, MA).

Hydrogen–deuterium exchange experiments

Borosilicate theta-capillaries (1.5 mm o.d. 1.0 mm i.d., Warner Instruments, Hamden, CT) were pulled with a P-87 pipette puller (Sutter Instrument, Novato, CA). The pulled tips (Fig. S-3) were measured with scanning electron microscopy (Sigma FE-SEM, Carl Zeiss Microscopy, Thornwood, NY). The capillaries were backfilled with 1 μM angiotensin I or 1 μM phenethylamine dissolved in 0.5 mM NaCl (H_2O), and 0.5 mM NaCl (D_2O), respectively. Choline and choline-d_9 at 1 μM concentrations were used as internal standards to monitor the relative flow between the two channels (Fig. S-2. The capillary was in turn mounted to a microelectrode holder with a conductive pin and pressure port (Warner Instruments, Hamden, CT) modified to hold a platinum wire. The microelectrode holder was in turn con-

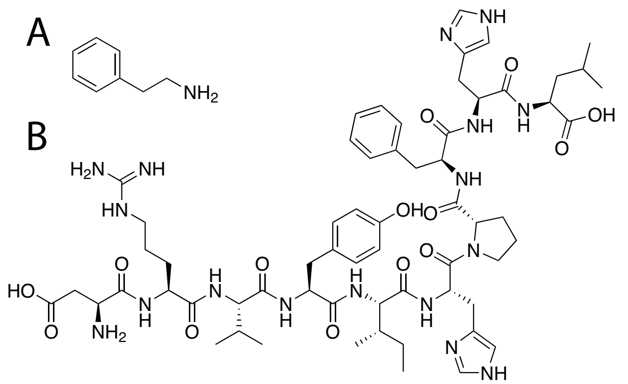

Figure S-1: Chemical structures of (A) phenethylamine and (B) angiotensin I.

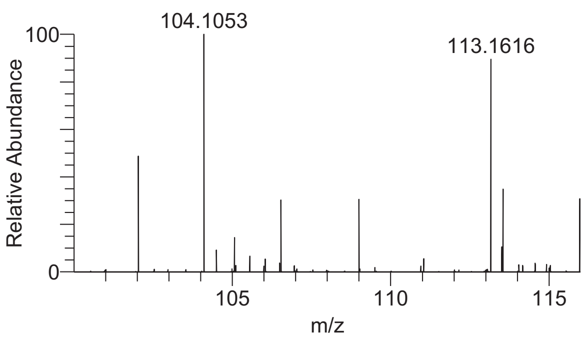

Figure S-2: Choline (*m/z* 104.105) and choline-d_9 (*m/z* 113.162) were used as internal standards to monitor the relative flow of the channels, found to be $\sim$ 1:1. The spectra were time-averaged across 1 min of data acquisition.

nected to the high-voltage source on the MS (the inlet was kept at ground potential) and N_2 gas at 10 psi. The microelectrode holder was operated with hydraulic micromanipulators (Narishige, East Meadow, NY). Mass spectrometry was performed with an LTQ-Orbitrap XL (Thermo Fisher Scientific, Waltham, MA). Mass spectra were acquired with detection in Orbitrap mode across *m/z* 100–750. The inlet capillary temperature was set to 275°C, spray voltage was 1 kV or 1.5 kV, with maximum injection time set to 500 ms per scan for analyte sampling. Measurements were done in triplicates. Spectral deconvolution was performed with MassWorks (Cerno Bioscience, Norwalk, CT). Data was further analyzed with MATLAB (Mathworks, Natick, MA) to obtain the rate constants from the systems of ordinary differential equations.

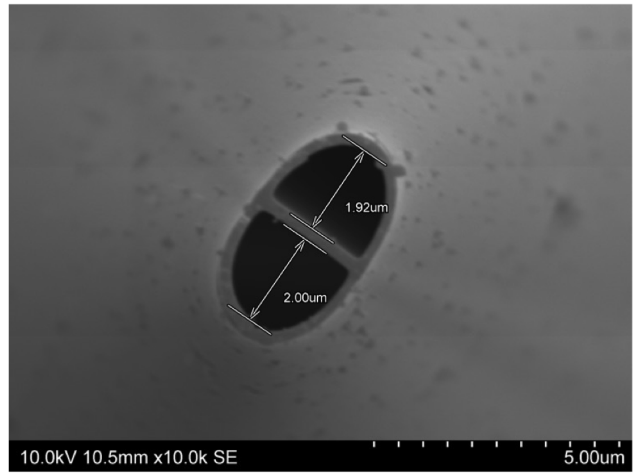

Figure S-3: Scanning electron microscopy was used to determine the tip size of the pulled theta-capillaries. The wall separating the two channels is $\sim$0.15 μm thick.

Micro-particle image velocimetry

Two pulsed second harmonic Nd:YAG lasers (MiniLase II, New Wave, Fremont, CA and DCR-11, Spectra Physics, Santa Clara, CA) with additional optics were used to set up the illumination system for particle imaging velocimetry. See figure S-4 for a schematic of the setup. By shifting the polarization direction of one laser beam using a half-wave plate, two laser beams were combined by passing a polarizing cube beamsplitter. A pair of irises was utilized to facilitate collineation of laser beams and coupling of lasers beams into a liquid light guide (Newport Model 77631). Coupling laser beams into a liquid light guide are advantageous for two reasons. First, it reduces the interference caused by diffraction patterns from the coherence of laser beams. Second, it allows more flexibility on the angle and position of illumination. The output beam from the liquid light guide was re-collimated using a pair of plano-convex lenses. Laser energy was fixed at 0.5 mJ. Pulse durations (FWHM) and jitters for MiniLase II and DCR-11 were 5$\pm$1 ns and 25$\pm$10 ns, respectively. Forward illumination was adopted. The angle of illumination was about 5° to the optical plane of the microscope objective. The time interval between two pulsed lasers was adjusted using a digital delay generator (DG535, Stanford Research Systems, Sunnyvale, CA). The timing of lasers was monitored using a photodetector (DET410, Thorlabs,

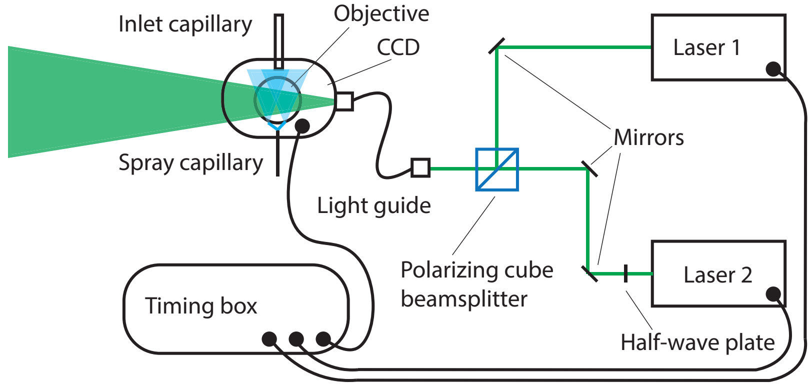

Figure S-4: Micro-PIV setup. The droplet size and velocities were interrogated with a dual Nd:YAG laser setup emitting light at 532 nm and an interline CCD.

Newton, NJ) connected to a digital oscilloscope (LT342, Teledyne LeCroy, Chestnut Ridge, NY). An interline-transfer CCD camera (MicroMAX, Princeton Instruments, Trenton, NJ) with a double image feature was used for rapid image acquisition (1 μs integration time per frame). The setup for electrospray was fitted into an inverted microscope using a 5x magnification, NA=0.15 objective with 13.6 mm free working distance (Plan-Neofluar, Axiovert 135, Carl Zeiss Microscopy, Thornwood, NY).We follow the suggestion of Meinhart et al., 2000 (ref. 29) to estimate the depth resolution (normal to optical plane) of the velocity measurements as follows:

$$\delta z_m = \frac{3n\lambda_0}{NA^2} + \frac{2.16 d_p}{\tan\theta} + d_p,$$

where n is the index of refraction, NA is the numerical aperture, λ_0 is the wavelength, and d_p is the geometric size of the particle.

The delay time between laser pulses between the two lasers was set to 500 ns, yielding one pulse per frame. Particle image data was acquired with WinView (Princeton Instruments, Trenton, NJ). Data was further analyzed with MATLAB (Mathworks, Natick, MA) using a cross-correlation algorithm (cf. Note 2) with ensemble averaged correlations of 25 image pairs per distance measured. Results are presented as a range of velocities corresponding to measured initial and final velocities in the field of view (denoting acceleration). The uncertainty of the time mean velocity was $\pm$7%. Computational fluid dynamics (CFD) modeling was performed with COMSOL Multiphysics (COMSOL AB, Stockholm, Sweden).

Note 1: Geometric characterization of the dual spray system and the resulting droplets

We observed that each channel forms its own Taylor cone–jet region (Fig. S-5). The borosilicate glass we used contains 81% SiO_2 and 13% B_2O_3, making it a good electric insulator. Because a 0.15 μm wall at the exit of the capillary separate both channels that carry the same polarity, it is reasonable that these two cone–jet regions should repel each other due to Coloumbic effects. However, we observed that $\sim$200 μm outside of the tip, the droplets from the two resulting sprays began to mix. The average size of the sprayed droplets were measured as 5$\pm$1 pixels, corresponding to on average d_p=4.3 μm in the range 1.3–6.1 μm. It should be noted that the lower boundary provides an upper estimate due to the point-response function that depends on the optical system and the wavelength of light being used for imaging. The following relation estimates the diameter of the point response function in the image plane (resulting from an ideal infinitesimal point of light):

$$d_s = \frac{1.22(1+M)\lambda}{NA}, \tag{1}$$

where λ is the wavelength, M is the magnification and NA is the numerical aperture of the objective. In our case, with M=5, λ=532 nm and NA=0.15, Eq. 1 gives d_s=26 μm. The final image that is recorded by the CCD can be estimated as a convolution of two Gaussian peaks resulting from the

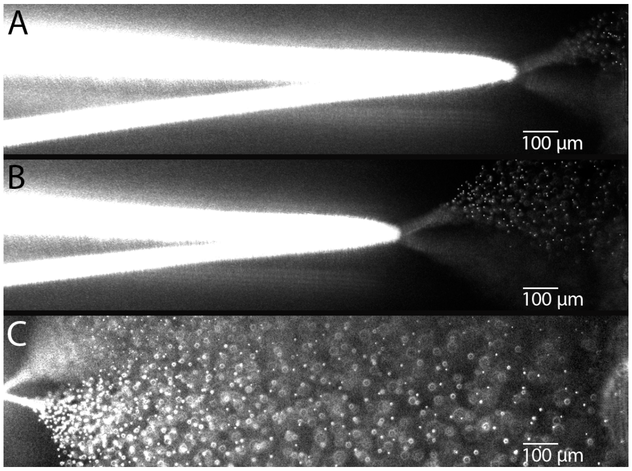

Figure S-5: Visualization of dual Taylor cone–jet regions breaking into droplets, obtained with nanoESI using theta-capillaries. Images were acquired with a ∼25 ns light pulse from an Nd:YAG laser at 532 nm. To enhance contrast for visualization, the intensity scale here is capped at 1000 units (acquired as 12-bit images). Two separate liquid jets repelling each other are observed. The mixing region where the droplets from the two resulting spray regions are found to start colliding with each other is located ∼0.2 mm from the tip of the theta-capillary. Distances between theta-capillary and inlet capillary were (A) d=0.32 mm (B) d=0.65 mm (C) d=1.77 mm. The bright smears spanning roughly 4/5 and 2/3 of the left side of images (A) and (B) are image artifacts resulting from light scatter from the theta-capillary.

point-response function and the particle diameter,

$$d_i = \sqrt{d_s^2 + d_p^2 M^2} \qquad (2)$$

where d_i is the image falling on the CCD, d_p is the geometric size of the particle. The physical size of the pixels on the used CCD array was 6.7 μm × 6.7 μm. As a result, for d_p less than ∼ 1.3 μm, d_s begins to be dominant in our system. Physical particle diameters less than 1.3 μm will be recorded as corresponding to physical diameters of about 1.3 μm (but with lower image intensity). In other words, all droplets of physical diameters of 1.3 μm or less will appear as 6.7 μm diameter images in the image plane and cover about 4×4 pixel areas.

Note 2: Determination of droplet velocity

To translate the measured distance between the theta-capillary and the MS-inlet into an average dwell time, we performed particle image velocimetry with two Nd:YAG lasers. This allowed us to obtain images of the droplets sprayed from the theta-capillary with Δt=500 ns between the frames. We measured and calculated velocity fields with an algorithm that calculates the cross-correlation between two frames in an image pair. For an image-pair with $n \times m$ pixels and an interrogation window with the size Δx and Δy, the cross-correlation is calculated as

$$R_{I_1 I_2}(\Delta x, \Delta y) = \\ = \sum_{x=0}^{n} \sum_{y=0}^{m} I_1(x,y) I_2(x+\Delta x, y+\Delta y).$$

As per Meinhart et al., 2000 (ref. 28), we perform ensemble time averages of these correlation functions in order to estimate time averaged velocities in each region of the 2D image. This gave the velocity of the sprayed droplets as a function of distance between the tip of the theta-capillary and the grounded capillary (Fig. S-6, Table 1).We found the droplets to accelerate 30% compared to their exit velocities in the direction toward the grounded capillary (Table 1). The average velocity **u** (parallel to the electric field) increased as a function of the electric field. These velocities were used to calculate the average dwell times used for kinetics by dividing the droplet travel distance between the beginning of the mixing zone and the MS inlet with the average velocities obtained from the velocity fields. The mixing of the two channels at the tip of the capillary is considered to be neglegible compared to droplet fusion mixing (Fig. S-7), because it is expected to only mix in 50 ppm of the components, compared to the 1:1 mixing that is observed after droplet fusion with mass spectrometry. The flow rates inside the capillaries were based on the exit velocity (the lower boundaries for **u** in Table 1) and tip channel size that was 2.00±0.18 μm (n=6, Fig. S-3), and were found to be in the range of 0.64–1.89 μl/min.

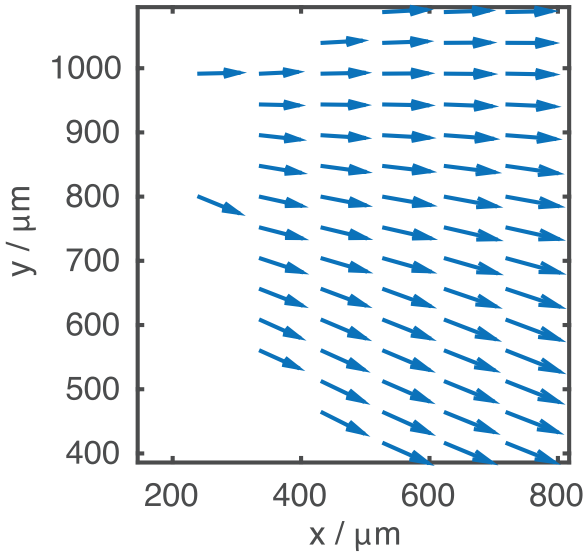

Figure S-6: Micro-particle image velocimetry provided measurements of in-plane velocity with components normal to the electric field (vertical direction in plot) and parallel to the electric field (horizontal). The applied voltage here was 1 kV and the backing pressure was 10 psi N_2. The vector plot shows measured velocity fields. Vector arrow lengths shown correspond to velocities from 14 to 17 m/s. The time between images used for these measurements was Δt = 500 ns. The velocity field corresponds to a physical region of 670 μm $\times$ 710 μm. At a distance of 0.87 mm from the spray capillary exit, the drops have accelerated to about 1.2 times their initial value.

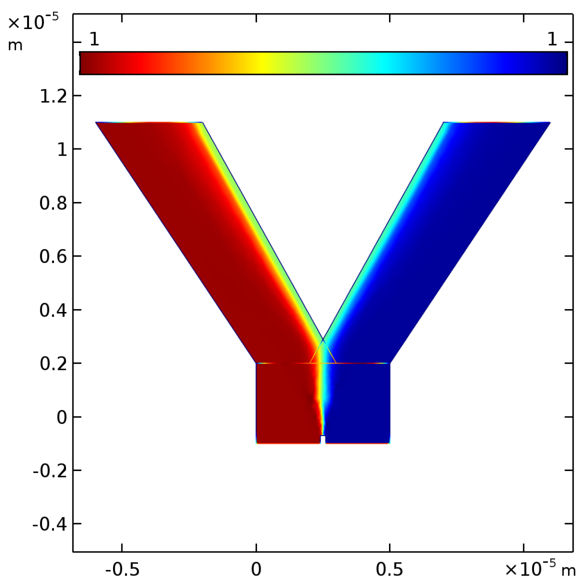

Figure S-7: Computational fluid dynamics model of the Taylor cone–jet region. Here the wetted interface between the two jets that repel each other due to Coulombic interaction is assumed to be similar to the size of the final droplets $\sim$ 4 μm. At the bottom the two liquids (H_2O and D_2O) exit the capillary tip capillary at 10 m/s. The fraction of channel 1 going into channel 2 and vice versa is $\sim$50 ppm. The inserted color bar at the top shows the relative mole fractions (red: 100% H_2O, blue: 100% D_2O).

Note 3: Mathematical model of hydrogen–deuterium exchange reactions

The deuteration of a compound with n exchangeable hydrogens can be described as a coupled reaction with forward and backward reaction rates k_i and k_{-i},

$RH_n \underset{k_{-1}}{\overset{k_1}{\rightleftharpoons}} RH_{(n\text{-}1)}D_1 \underset{k_{-2}}{\overset{k_2}{\rightleftharpoons}} RH_{(n\text{-}2)}D_2\cdots$

$\ldots RH_1D_{n\text{-}1} \underset{k_{-(n-1)}}{\overset{k_{(n-1)}}{\rightleftharpoons}} RD_n$. The reaction can be described as a system of ordinary differential equations in matrix-form,

$$\mathbf{x}' = \mathbf{A}\mathbf{x},$$

where $\mathbf{x}'$ is the time-derivative of each species, $\mathbf{A}$ is the coefficient matrix containing the forward and backward reaction rates k_i and k_{-i} and $\mathbf{x}$ is the concentration of each specie as a function of time. In expanded form, the equation is written as:

$$\begin{bmatrix} x_1' \\ x_2' \\ x_3' \\ \vdots \\ x_n' \end{bmatrix} = \begin{bmatrix} -k_1 & k_{-1} & 0 & 0 & \dots & 0 & 0 \\ k_1 & -(k_{-1}+k_2) & k_{-2} & 0 & \dots & 0 & 0 \\ 0 & k_2 & -(k_{-2}+k_3) & k_{-3} & \dots & 0 & 0 \\ \vdots & \vdots & \vdots & \vdots & \ddots & \vdots & \vdots \\ 0 & 0 & 0 & 0 & \dots & k_{(n-1)} & -k_{-(n-1)} \end{bmatrix} \begin{bmatrix} x_1 \\ x_2 \\ x_3 \\ \vdots \\ x_n \end{bmatrix}.$$

Note 4: Mathematical model of convective evaporation of a droplet travelling in air

According to Holterman, 2003 (ref. 31), the rate of decrease of the diameter D of a water droplet travelling in air can be described using the Ranz–Marshall correlation:

$$\frac{dD}{dt} = \frac{-4M_L D_{v,f}}{D\rho_L RT_f}\Delta p\left(1+0.276\mathrm{Re}^{1/2}\mathrm{Sc}^{1/3}\right),$$

where Re is the Reynolds number, Sc is the Schmidt number, $D_{v,f}$ is the average diffusion coefficient for vapor molecules and T_f is the average absolute temperature in the saturated air immediately surrounding the drop, M_L is the molecular weight of the evaporating liquid, ρ_L is the liquid density, Δp is the difference between the vapor pressure near the drop (the saturation pressure) and the partial pressure of vapor far from the drop, and R is the gas constant. The Reynolds number is

$$\mathrm{Re} = \frac{\rho_{a,f} D v}{\eta_{a,f}},$$

where v is the droplet velocity, $\rho_{a,f}$ and $\eta_{a,f}$ are the air density and viscocity at temperature T_f.The Schmidt number is

$$\mathrm{Sc} = \frac{\eta_{a,f}}{\rho_{a,f} D_{v,f}}.$$

The Ranz–Marshall correlation holds for $\mathrm{Re} \in [0,200)$ and $\mathrm{Sc} \in [0,250)$. For our experiments $\mathrm{Re} \in [1,10]$ and $\mathrm{Sc} = 0.6$, making the correlation valid for our system.

We solved the differential equation numerically given physicochemical properties of water and air at ambient conditions, and room temperature (20°C). Figure S-8 shows the solutions to the differential equation solved for a droplet with a 4.3 μm initial diameter travelling at v_1=22 m/s, v_2=11 m/s or v_3=8 m/s.

In our HDX experiments the droplet travel time in air was t_1 ∼20 μs for the highest velocity and t_2 ∼320 μs for the lowest velocity. As a result, the droplet diameter is expected to have decreased by ∼0.1–1.2%

before entering the inlet, which at most results in a reduction of the droplet volume by 3.6%.

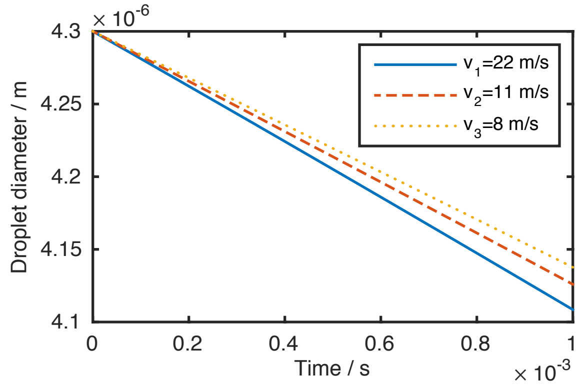

Figure S-8: Droplet size as a function of travel time in air due to convective evaporation under ambient conditions and room temperature (20 °C). The solutions for the differential equations are shown for v_1=22 m/s, v_2=11 m/s and v_3=8 m/s.